University of Huddersfield Repository

Grossoni, Ilaria, Iwnicki, Simon, Bezin, Yann and Gong, Cencen

Dynanics of a vehicle-track coupling system at a rail joint

Original Citation

This version is available at http://eprints.hud.ac.uk/id/eprint/22817/

http://eprints.hud.ac.uk/

DYNAMICS OF A VEHICLE-TRACK COUPLING SYSTEM AT RAIL JOINT

Ilaria Grossoni[1], Simon Iwnicki[1], Yann Bezin[1] and Cencen Gong[1]

Abstract

The dynamic behavior at a rail joint is examined using a two-dimensional vehicle-track coupling model. The track system is described as a finite length beam resting on a double layer discrete viscous-elastic foundation. The vehicle is represented by a half car body and a single bogie. The influence of the number of track layers considered, the number of rail elements between two sleepers and the beam model type is investigated. Parametric studies both of the coupling model and the analytic formulae are carried out in order to understand the influence of the main track and vehicle parameters on the P1 and P2 peak forces. Finally, the results in terms of P2 force from the present model have been compared not only with measured values but also with other simulated and analytical solutions. An excellent agreement between simulated and measured values has been found and the variation with respect to analytical formulae has been quantified.

Keywords

Rail joints, vehicle-track interaction, dynamic behaviour, P1 force, P2 force

Introduction

When a train runs over a joint, large dynamic impact forces are developed which lead to vibrations in the structures and a higher probability of component fatigue and damage. Thus, it is clear that rail joints can affect the maintenance costs, ride comfort and running security on a modern railway.

Although there is currently a worldwide trend towards using continuously welded rails to minimize the wheel-rail impact forces rail joints are still common in some areas. For example, insulated rail joints are required for track electrical insulation to detect the train location and to isolate sections such as those near road crossings.

Many studies have focused on the dynamic response of the railway track under moving vehicles. Some of these [1-3] only consider the track system as a beam on an elastic foundation subjected to moving point loads. Although this approach is simple to implement, it is insufficient to fully model the dynamic behavior of the track and vehicle systems as it neglects

the wheel-rail contact aspects. Some other studies [4-7] take the coupling aspects into account, but only a few [8, 9] apply these aspects to model the dynamic behaviour with a rail joint.

In this paper, a two-dimensional vehicle-track coupling model is established. The track system is described as a finite length beam supported on a two-layer discrete elastic foundation. The vehicle is represented using a half car body. These sub-systems are solved independently and coupled together through a Hertzian wheel-rail contact model [4], where the irregularity due to the rail joint is modelled as a second order polynomial. The influence of number of layers considered, the number of elements between two sleepers and the beam model is investigated. An extensive parametric study has been carried out through both the FE model established and the analytical formulae, through which it is possible to point out the differences using a predictive model and an analytical one. The main results have shown that the first impact force P1 is greatly influenced by the wheelset mass, the rail mass and the joint angle, whereas the second peak force P2 is largely affected by the wheelset mass, the rail-pad stiffness, the support stiffness and the joint angle. The parametric study from the analytic formulae demonstrates the robustness of the coupling model established. Finally, the results in terms of the P2 force from this model have been compared with measured data [8], another simulated model [8] and analytical solutions [10, 11]. An excellent agreement has been found with measured data and the simulated model.

Modelling the vehicle-track coupling system

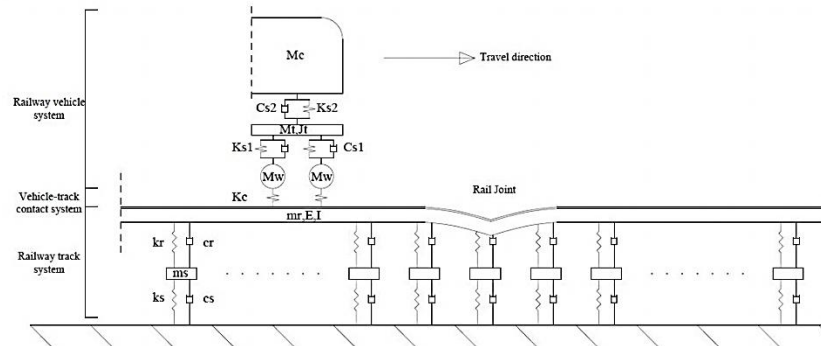The vehicle-track coupling model with a rail joint is shown in Figure 1.

Figure 1. Vehicle-track coupling model with a rail joint (Mc: car-body mass; Ks2: secondary suspension stiffness; Cs2: secondary suspension damping; Mt: bogie mass; Jt: bogie pitch moment of inertia; Ks1: primary suspension stiffness; Cs1: primary suspension damping; Mw: wheelset mass; Kc: contact stiffness; mr: rail mass per unit length; E: rail Young's modulus; I: rail inertia; kr: rail-pad stiffness; cr: rail-pad damping; ms: sleeper mass; ks: support stiffness; cs: support damping).

Fundamental assumptions

The main assumptions are listed:

1) Only vertical dynamic forces are considered. Due to the track symmetry, it is possible to consider a single rail in the calculation.

2) The track system is modelled through a two-layer discretely supported ballast track model. A finite straight track without imperfections is considered. The number of beam elements considered is 90, because in this way it is possible to avoid the overlapping between the increasing static load during the transient time and the dynamic forces due to the rail joint.

3) A half car body is considered for the vehicle model. All the masses are assumed to be concentrated at the centre of gravity of the corresponding element. The two wheelsets masses and profiles are assumed to be the same.

4) The non-linear Hertzian contact model is used to couple the vehicle and track models. It is assumed also that there is one contact point at each wheel.

5) An iterative scheme has been used in order to solve the coupling problem.

Modelling the track system

A finite element (FE) analysis is developed approximating the deformation within an element using nodal values of displacement and rotation. The third order Hermitian interpolation is assumed to be valid in this study.

The Euler-Bernoulli mass, stiffness and damping matrices of the generic i-th element are reported in Appendix 1.

The moving force is characterized by a constant value of speed V. Thus the simple formula for the uniform linear motion has been used.

Modelling the vehicle system

The model used here consists of half car supported by a bogie through the secondary suspension and a bogie supported by two half wheelsets through the primary suspension. All the bodies are assumed to be rigid.

The vehicle mass, stiffness and damping matrices are reported in Appendix 2.

Modelling the irregularity

A quadratic function can be used to describe the deformed shape of the rail, as highlighted from the comparison with the measurements shown in [12].

It has been assumed that at the start and final point of the joint the first derivate of the function is equal to zero.

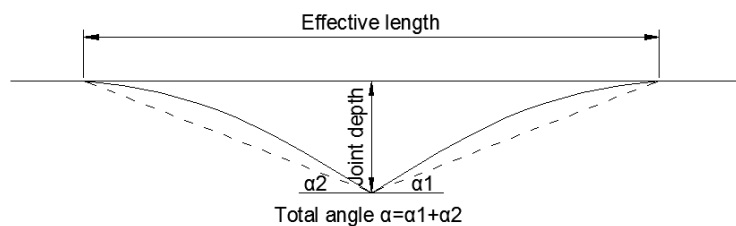In Figure 2 the idealised form of the joint used in the model is presented.

Figure 2. The joint idealised form used in the model (irr(x): irregularity value at point x) [10]. The dotted lines are the geometrical constructions for the calculation of the effective length.

The quadratic function describing the irregularity irr(x) can be established as

$$irr(x) = \begin{cases} \dfrac{4D}{L^2}x^2 & 0 \leq x \leq \dfrac{L}{2} \\ \dfrac{4D}{L^2}\left(x - \dfrac{L}{2}\right)^2 - \dfrac{4D}{L}\left(x - \dfrac{L}{2}\right) + D & \dfrac{L}{2} \leq x \leq L \end{cases}$$

Where D is the maximum depth of rail joint and L the effective length of the rail joint. In particular, the length of rail joint L is defined as the sum of horizontal projection of the tangential lines which start from the dip bottom and have the inclination equal to, respectively, α1 and α2.

Results

In order to solve the coupling system, the parameters used are reported in [13].

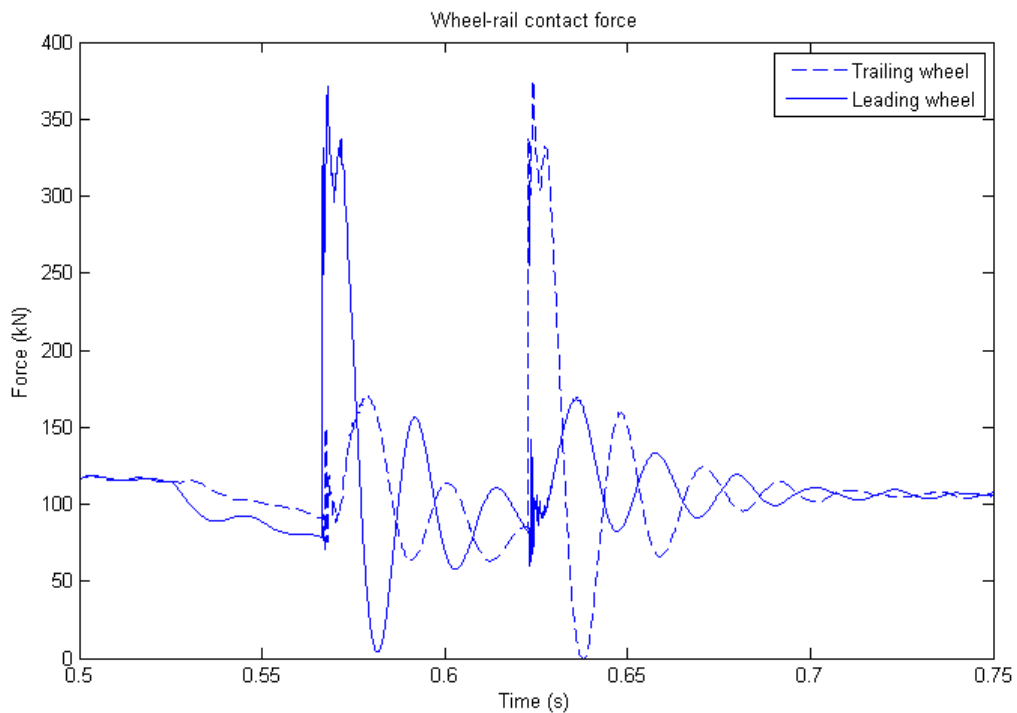The response in terms of wheel-rail contact force versus time is shown in Figure 3.

Figure 3. Wheel-rail contact force versus time: leading and trailing wheels.

In Figure 4 the displacement and the acceleration of the central node and in central sleeper (45th sleeper) are presented. The two peaks are due to the passage of each of the two wheelsets, which occurs respectively at 0.56 and 0.63 seconds. Due to the energy connection between the leading and the trailing wheelset, the second peaks in all the physical quantities shown, including the wheel-rail contact force and the rail acceleration, are larger than the first ones.

(a)

(b)

(c)

(d)

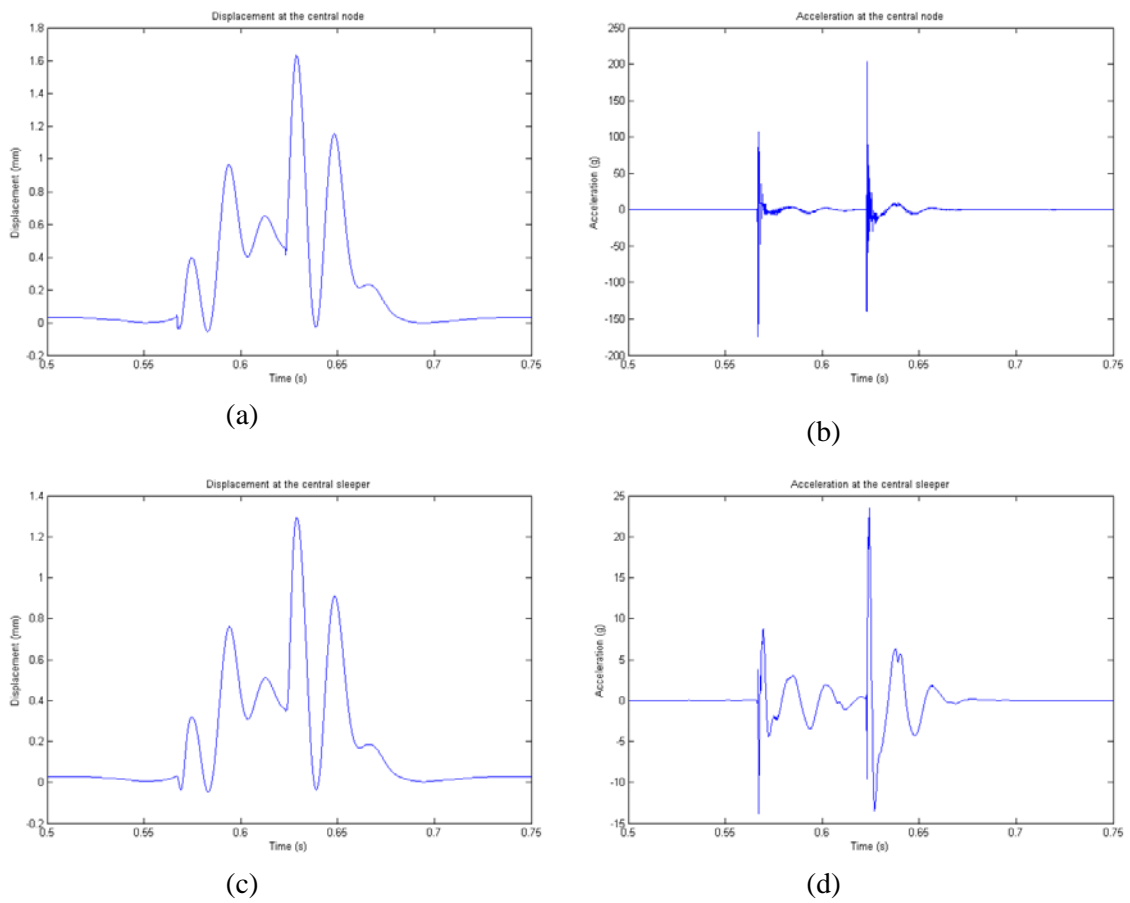**Figure 4.** (a) Rail displacement at the central node versus time; (b) Rail acceleration at the central node versus time; (c) Mid-sleeper displacement versus time; (d) Mid-sleeper acceleration versus time.

In Figure 5 the comparison between models (i.e. two- and three-layer model) and different beam types (i.e. Euler-Bernoulli and Timoshenko beam) both in time domain and frequency domain is presented.

Figure 5(a) shows that the first peak value is the same passing from 2-layer to 3-layer model, whereas the shape is not conserved. This is because the foundation stiffness has not been changed accordingly.

Adding a layer which represents the ballast mass affects the results as the larger inertia leads to a shift of the two characteristic peaks in the frequency domain (Figure 5(b)).
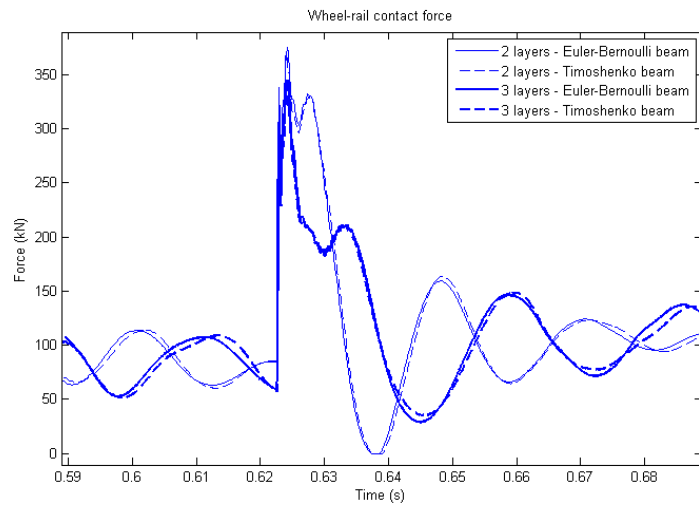
(a)

(b)

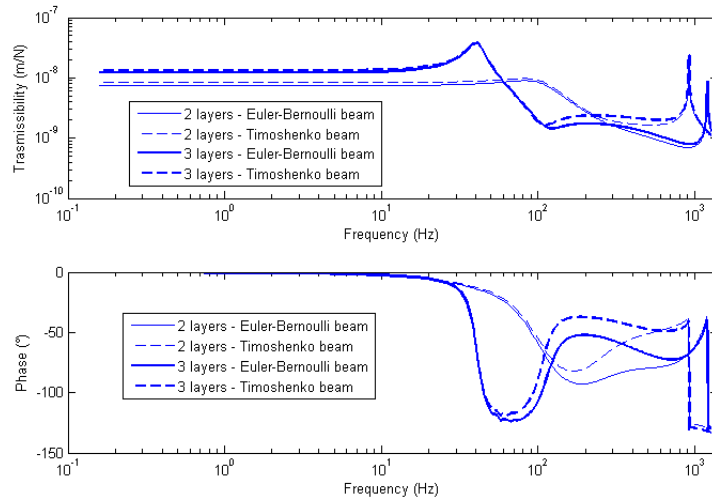**Figure 5.** Comparison between models (two and three layers) and different beam types (Euler-Bernoulli and Timoshenko beam) in (a) time domain and (b) frequency domain (central sleeper).

In Figure 6 the comparison in terms of number of elements in a sleeper bay is shown. The model used for that is the two-layer discretely supported ballast track with Euler-Bernoulli beam. As expected, the more elements that are considered, the more stable the results and less oscillations are presented. It is worth noticing that when the number of elements more than 4 the differences are negligible, also in terms of maximum peak force.

On the other hand, increasing the number of elements leads to an increasing of computational costs. As an example, the running times required[1] in each case and the maximum forces are presented in Table 1.

Table 1. Comparison between different models in terms of running time required and maximum force.

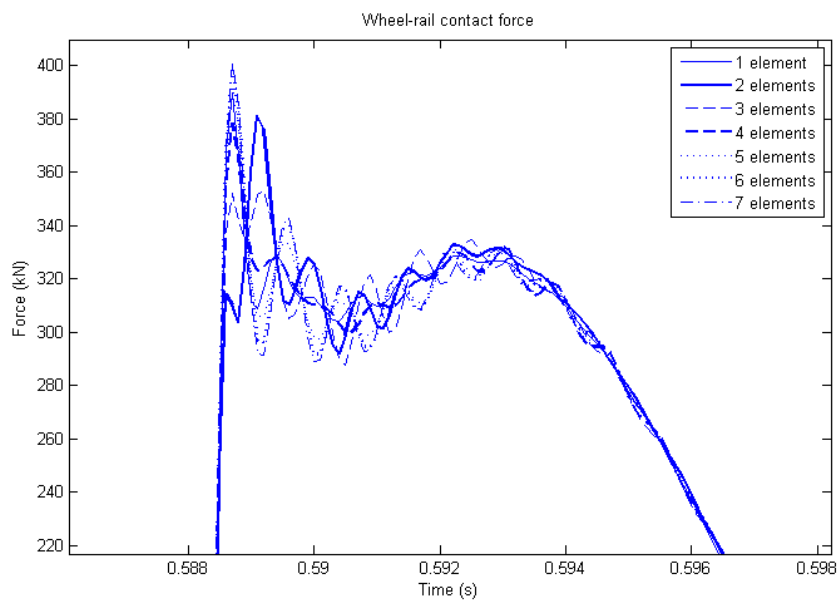| N. elements	1	2	3	4	5	6	7
Running time (s)	75.5	199.9	400.8	728.21	1223.7	1917.3	2315.1
Maximum force (kN)	375.1	389.7	387.7	385.8	384.7	383.7	383.0

Figure 6. Wheel-rail contact force depending on the number of elements between two sleepers (two-layer model; Euler-Bernoulli beam).

---

[1] The PC used for the simulation is an Intel(R) Core(TM) i7-3770 with 16GB RAM.

Analysing Figure 3, it is also possible to recognize two peak forces, frequently called P1 and P2 forces.

The P1 force is a high frequency peak force (approximately 500-1000 Hz) characterized by a high magnitude approximately five times higher than the unsprung static load [10]. It is associated mainly to the battering of the unsprung mass on the rail-end and is absorbed mainly by the rail and sleeper inertias. In the example shown in Figure 2, the force peak occurs 0.3 ms after crossing the joint, which is within the typical range between 0.25 ms and 0.5 ms [10].

The P2 force, which occurs several milliseconds after the impact, is a medium frequency force (approximately 30-100 Hz) and its peak is lower than the P1, around three times higher than the static force [10]. Contrary to the P1 force, the P2 force depends on the rail bending resilience and it is transmitted to the ballast, producing an acceleration of deterioration of the whole track system, in particular ballast settlement. The dynamic force transmitted depends principally on the unsprung masses, while the other primary and secondary suspended masses are well isolated to such short duration peak loads. This is the reason why vehicle designers are striving to reduce unsprung masses as much as possible.

The P1 and P2 forces can be determined in the first approximation as in equations (1) and (2) [10]

$$P_1 = P_0 + 2\alpha V \sqrt{\frac{K_H m_e}{1 + \frac{m_e}{m_u}}} \tag{1}$$

$$P_2 = P_0 + 2\alpha V \cdot \left(1 - \frac{c_t \pi}{4 k_t (m_t + m_u)}\right) \cdot \sqrt{\frac{1}{1 + \frac{m_t}{m_u}} \cdot k_t m_u} \tag{2}$$

Where P_0 is the static wheel load (N), 2α the total joint angle (rad), V the travelling speed (m/s), K_H the linearized Hertzian contact stiffness (N/m) as defined in [10], m_u the vehicle unsprung mass (kg), m_e the effective track mass (kg) and m_t, k_t and c_t the equivalent track system parameters defined in [10].

The UK standard GM/TT0088 states that "vehicles shall be able to run over the normal range of vertical track irregularities at normal operating speeds without generating excessive vertical

loads and stresses in the rails and track" [11]. There is a limit only for the P2 force, which cannot exceed a total value of 322 kN per wheel at the maximum operative speed. This limit is made because this force is directly transmitted to the ballast, as said previously. In particular, an analytical formula has been proposed in equation (3) by [11]

$$P_2 = Q + A_z \cdot V_m \cdot M \cdot C \cdot K \tag{3}$$

Where Q is the maximum static wheel load (N), Az the total angle of vertical ramp discontinuity, fixed to 0.02 rad, V_m the maximum normal operating speed (m/s), M_v the effective vertical unsprung mass per wheel (kg), M, C and K parameters reported in [11]. As pointed out in [14], "although the concept of effective unsprung mass is simple, its accurate evaluation is not always straightforward".

Parametric study of the FE model

Numerical examples are shown and the effects of some parameters are investigated. The parameters of track, vehicle and joint models which have been used in the simulation are reported in Table 2.

Table 2. Parameters used in the simulation.

	Track model	Vehicle model	Joint model
Parameters	Travelling speed S	Travelling speed S	Travelling speed S
	Rail mass per unit length $\overline{m}_r$	Wheelset mass M_w	Affected length L
	Rail-pad stiffness k_r	Bogie mass M_t	Total joint angle 2α
	Support stiffness k_s	Car body mass M_c	
	Total joint angle 2α	Total joint angle 2α	

In the following, only the most relevant graphs are reported.
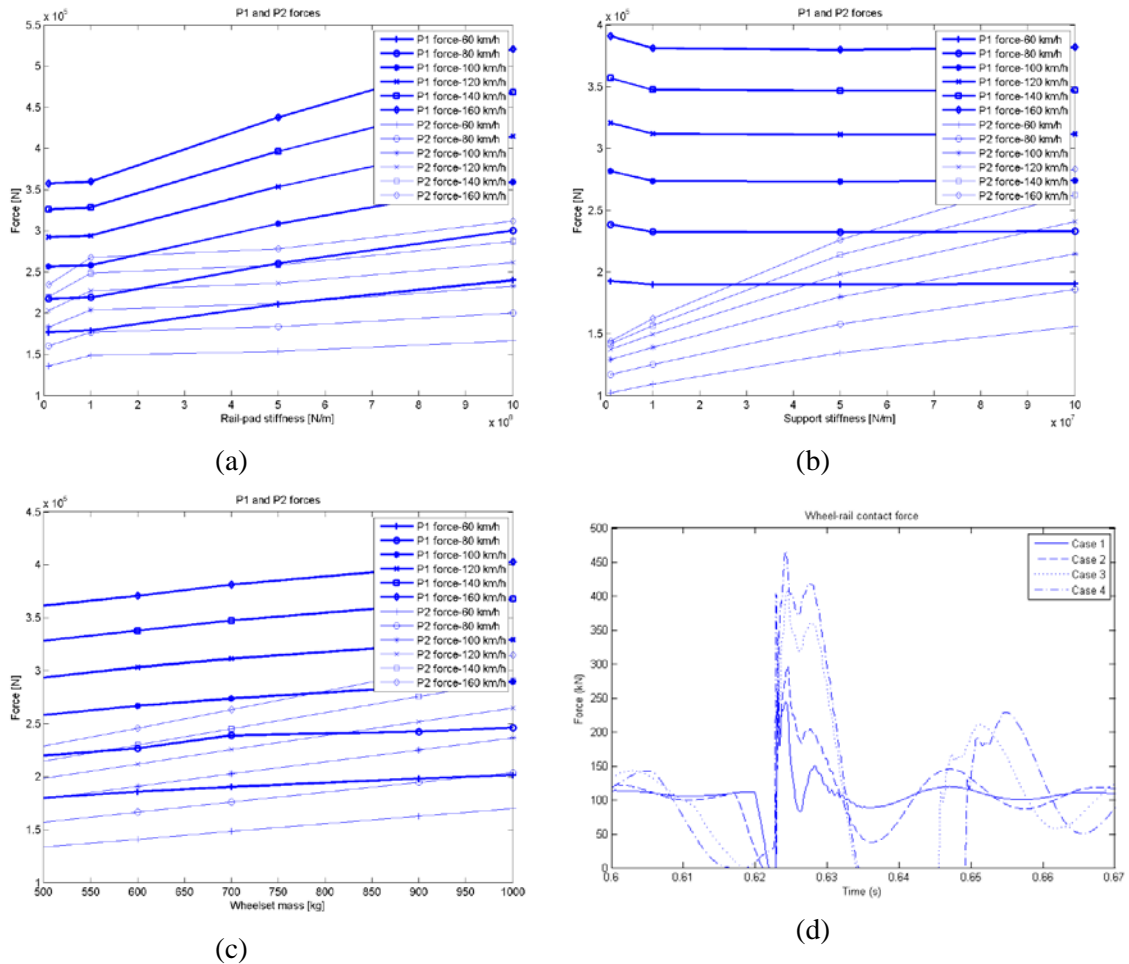
(a)

(b)

(c)

(d)

Figure 7. The variation of P1 (bold lines) and P2 (normal lines) forces with (a) rail-pad stiffness; (b) support stiffness; (c) wheelset mass; (d) joint shape fixing the total joint angle to 25 mrad (Case 1: joint depth equal to 1 mm and effective length equal to 0.25 m; Case 2: joint depth equal to 2 mm and effective length equal to 0.5 m; Case 4: joint depth equal to 4 mm and effective length equal to 1 m; Case 4: joint depth equal to 6 mm and effective length equal to 1.5 m).

From Figure 7(a), it is found that the trends of P1 and P2 forces with the rail-pad stiffness are different. In the case of P1 force, there is a first constant trend for low stiffness values (10-100 MPa) and then a linearly increasing trend for higher stiffness (500-1000 MPa). The slope increases with increasing speed. In case of P2 force, instead, there is a relatively rapid increasing trend for low stiffness values (10-100 MPa) and then a relatively slower increasing trend for higher stiffness (500-1000 MPa) with a slope significantly lower than the first part.

Regarding the support stiffness (Figure 7(b)), it can be found that the P1 trend is relatively constant while the P2 grows more than linearly. The average slope increases with increasing travelling speed. This means that decreasing the ballast stiffness has little effect on the P1 force, whereas it can reduce the P2 force.

As shown in Figure 7(c), the impact of the wheelset mass is very large in both cases. In particular, the P1 force trend is asymptotic, that is the change of wheelset mass plays a limited role in that impact force for values greater than 600-800 kg. The P2 force increases proportionally with the wheelset mass, with the average slope increasing with increasing travelling speed.

Finally, from Figure 7(d) it can be deduced that both the impact forces are different in case of different effective length, even if the joint angle is fixed to 25 mrad. Thus, the dynamic response in terms of wheel-rail contact forces is closely related to the actual shape of the rail joint under loading. This conclusion is against the formulae proposed by the UK researchers in equations (1) and (2), according to which the forces are constant for constant value of total dip angle.

Parametric study of the analytical model

A parametric study has been performed also using the analytic models in equations (2) and (3) from [10] and [11] respectively.

For the former model, the parameters used in the simulations are six: the travelling speed V, the foundation stiffness k_t, the joint angle α_t, the rail section properties (mass per unit length m and inertia I) and the unsprung mass Mu. For the latter model, on the contrary, the parameters used are three: the travelling speed V, the maximum static wheel load and the unsprung mass Mu. In fact, in this case all the other parameters regarding the track properties, both rail and support, are fixed equal to typical values.
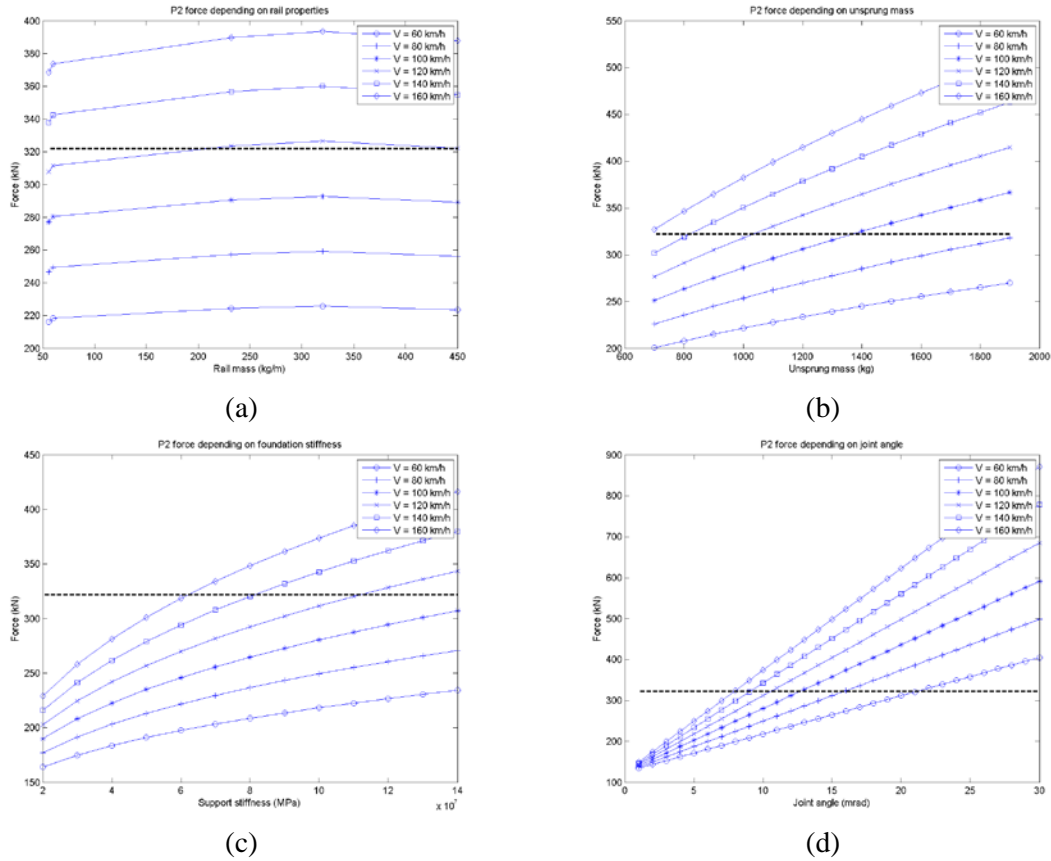
Figure 8. Variation of P2 force with (a) rail mass (m); (b) unsprung mass (Mu); (c) foundation stiffness (kt); (d) joint angle (α_t) using equation (2) varying the travelling speed (V). The dashed line represents the P2 force limit according to [11].

From Figure 8(a) it can be found that there is a relatively rapid increasing trend for smaller profiles (50-60 kg/m) and then a relatively slower increasing trend for bigger profiles (60-320 kg/m) with a slope significantly lower than the first part. Finally, increasing the rail profiles beyond values around 320kg/m leads to a decrease of the peak force.

All figures show that there is an increasing impact of the unsprung mass on the P2 force with increasing the travelling speed. This trend is the same found with the FE model (Figure 7(c)).

Figure 8(b) show that the unsprung mass has a strong influence on the P2 peak force.

As shown in Figure 8(c), the influence of the support stiffness is very large. The increasing trend is reasonably linear in case of low speeds (60-80 km/h) and the slope rises with increasing

speed. In case of higher speeds (120-160 km/h), on the contrary, the growth is more than linear, as found in Figure 7(b).

Finally, from Figure 8(d) it can be deduced that the joint angle plays an important role for the impact force level, as expected. The variation of the P2 force is linear and the average slope increases with increasing speed.
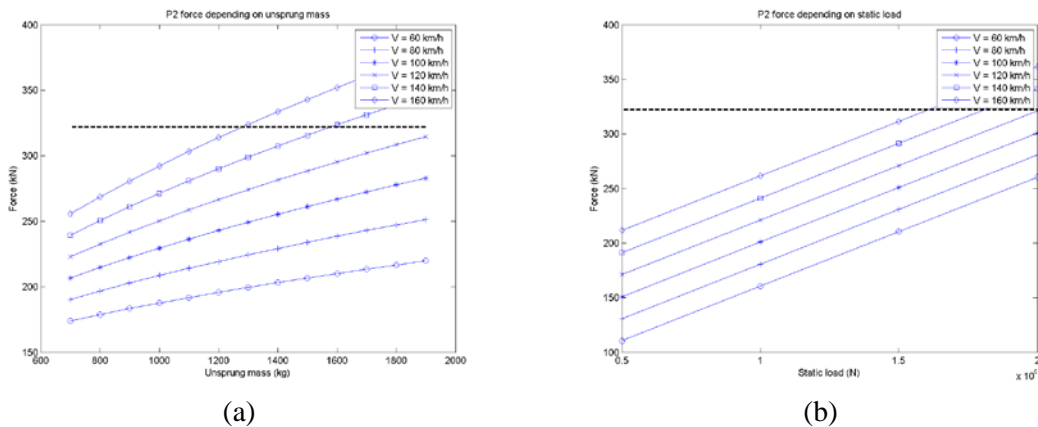

(a)   (b)

Figure 9. Variation of P2 force with (a) unsprung mass (Mu); (b) maximum static wheel load (Load) using equation (3) varying the travelling speed (V). The dashed line represents the P2 force limit according to [11].

As found from Figure 8(b), the variation of the impact force with the unsprung mass is linear and the slope increases with increasing speed (Figure 9(a)).

Figure 9(b) shows that there is a linear increasing of the P2 force with the static load, as expected from equation (3).

To conclude, it is worth remarking that the FE model established reproduces the same trends found applying the well-known analytic formulae in equations (2) and (3) (Figure 8 and Figure 9) and also allows other important factors to be taken into account with a relative low running time cost (Table 1).

Comparison

The present FE model has been compared with the above analytical models and reference from the literature. The analysis reported in [8] has been used based on measurements for two different Chinese freight vehicles. The main characteristics of two different freight vehicles, C62A and C75, are reported in [8].

In Figure 10 the comparison between the results in terms of P2 force in case of C62A and C75 freight vehicles with increasing travelling speed is shown. In particular, for each travelling speed and each vehicle type five different values of the peak force are considered: measured data [8], simulated value [8], two different analytic solutions [10, 11] and the present model.
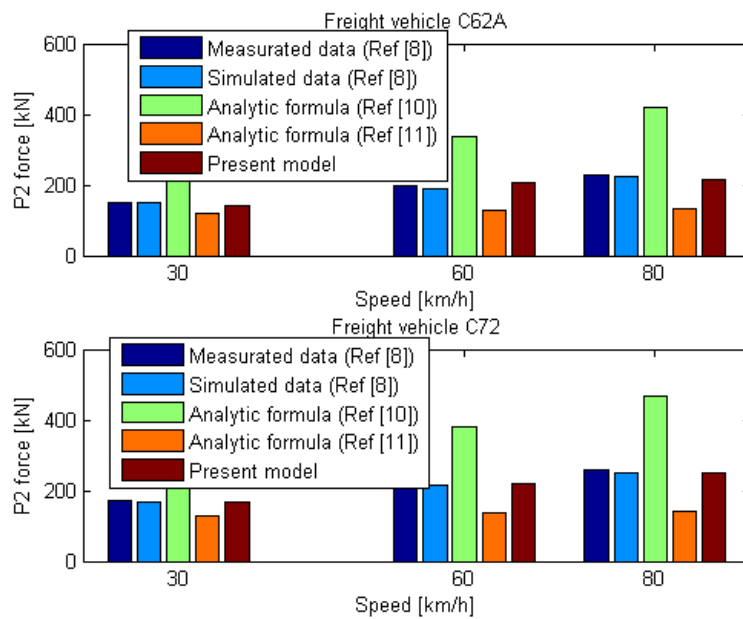

Figure 10. Comparison between the results in terms of P2 force in case of C62A and C75 freight vehicles.

Figure 10 shows that in this case the analytic formula in [10] overestimates the peak force whereas the one in [11] underestimates it. This can be explained remembering that in the latter case the track parameters, including the mass, stiffness and damping properties, are fixed.

It is noticeable that the results are close to each other, particularly the measured data, simulated values and the present model. The percentage differences between the present model and measured data or simulated values are reported in Table 3.

Table 3. Percentage differences between the present model and measured data [8] or simulated values [8].

Travelling speed [km/h]	C62A		C75	
	Measured data (%)	Simulated values (%)	Measured data (%)	Simulated values (%)
30	4.5	3.2	3.2	0.8

60	3.7	10.9	2.2	1.6
80	6.5	4.4	3.7	0.6

Conclusions

The primary objective of this study was to investigate the characteristics of vertical dynamic response at a rail joint using a comprehensive FE model of vehicle-track coupling system. The two dimensional model employed has been established by merging iteratively three elementary models, which are the track model, the vehicle model and the contact model. This strategy was proven efficient to obtain the numerical solution in time domain. In order to achieve a reasonable model size which is compatible to the available computing facility, several assumptions have been made in the rail joint model, track model and boundary conditions.

The wheel-rail impact mechanism can be explained through the stiffness discontinuity of the joint structure. At impact, two peak contact forces develop. The main characteristics, such as the frequency and the magnitude, are quite different. It has been demonstrated that the lower magnitude force is the force that actually causes the track degradation because its characteristic frequencies match with the track frequencies.

Through a series of sensitivity studies of several parameters, it has been shown that the dynamic response can be largely improved by optimised design parameters. The parametric simulations have shown that the first impact force P1 is greatly influenced by the wheelset mass, the rail mass and the joint angle, whereas the second peak force P2 is affected by the wheelset mass, the rail-pad stiffness, the support stiffness and the joint angle. The model has outlined that the impact forces depends on the actual shape of the rail joint. Therefore, great reductions of peak forces values can be obtained through an appropriate joint design.

The parametric study from the analytical formulae has pointed out that the FE model established in this study can reproduce the same trends and also allows other important factors to be taken into account with a relative low running time cost.

Finally, the results in terms of P2 force from the present model have been compared not only with measured values but also with both simulated and analytical solutions. An excellent agreement between values has been found, with a maximum percentage difference of 10%.

Acknowledgements

References

1. Thambiratnam, D. and Y. Zhuge, *Dynamic analysis of beams on an elastic foundation subjected to moving loads.* Journal of Sound and Vibration, 1996. **198**(2): p. 149-169.
2. Wang, Y., et al., *Transient responses of beam with elastic foundation supports under moving wave load excitation.* International Journal of Engineering and Technology, 2011. **1**(2): p. 137-143.
3. Grassie, S.L., et al., *The Dynamic Response of Railway Track to High Frequency Vertical Excitation.* Journal of Mechanical Engineering Science, 1982. **24**(2): p. 77-90.
4. Lei, X. and N.A. Noda, *Analyses of dynamic response of railway track to high frequency vertical excitation.* Journal of Sound and Vibration, 2002. **258**(1): p. 147-165.
5. Zhai, W., K. Wang, and C. Cai, *Fundamentals of vehicle–track coupled dynamics.* Vehicle System Dynamics, 2009. **47**(11): p. 1349-1376.
6. Lu, F., et al., *Symplectic analysis of vertical random vibration for coupled vehicle–track systems.* Journal of Sound and Vibration, 2008. **317**(1–2): p. 236-249.
7. Diana, G., et al., *Modelli matematici per lo studio della interazione veicolo-struttura-armamento.* Ingegneria ferroviaria, 1995(12).
8. Zhai, W. and Z. Cai, *Dynamic interaction between a lumped mass vehicle and a discretely supported continuous rail track.* Computers & Structures, 1997. **63**(5): p. 987-997.
9. Dukkipati, R.V. and R. Dong, *The Dynamic Effects of Conventional Freight Car Running over a Dipped-joint.* Vehicle System Dynamics, 1999. **31**(2): p. 95-111.
10. Jenkins, H.H., et al., *The effect of track and vehicle parameters on wheel/rail vertical dynamic forces.* Railway Engineering Journal, 1974. **3**(1): p. 2-16.
11. British Railways Board, *Permissible track forces for railway vehicles*, 1993, Group Standards Railway Technical Centre: Derby.
12. Wu, T.X. and D.J. Thompson, *On the impact noise generation due to a wheel passing over rail joints.* Journal of Sound and Vibration, 2003. **267**(3): p. 485-496.
13. Grossoni, I., et al. *Dynamic response of vehicle-track coupling system with an insulated rail joint.* in *11th International Conference on Vibration Problems (ICOVP-2013).* 2013. Lisbon.
14. RSSB, *A review of dynamic vertical track forces*, 2002.

Appendix 1

In order to establish the mass matrix for the generic i-th element, it is necessary to integrate the vibrational kinetic energy expressing the squared speed of rail displacement at the point x in terms of nodal displacements thought the Hermitian interpolation. Therefore

$$[m]_i = \frac{\bar{m}_r l}{420} \cdot \begin{bmatrix} 156 & 22l & 54 & -13l \\ 22l & 4l^2 & 13l & -3l^2 \\ 54 & 13l & 156 & -22l \\ -13l & -3l^2 & -22l & 4l^2 \end{bmatrix}$$

Where $\bar{m}_r$ is the rail mass per unit length (kg/m) and l the element length (m).

The stiffness matrix of the generic i-th element is formed by two contributions, i.e. the contribution from the rail $[k]_i^r$ and the contribution from the rail-pad $[k]_i^{rp}$. Similarly to the previous case, the first part is calculated integrating the bending strain energy and expressing the rail displacement in terms of nodal displacement. The second part, on the contrary, is concentrated.

Thus

$$[k]_i = [k]_i^r + [k]_i^{rp} = \frac{EI}{l^3} \cdot \begin{bmatrix} 12 & 6l & -12 & 6l \\ 6l & 4l^2 & -6l & 2l^2 \\ -12 & -6l & 12 & -6l \\ 6l & 2l^2 & -6l & 4l^2 \end{bmatrix} + k_r \cdot \begin{bmatrix} 1 & 0 & 0 & 0 \\ 0 & 0 & 0 & 0 \\ 0 & 0 & 1 & -0 \\ 0 & 0 & 0 & 0 \end{bmatrix}$$

Where EI is the beam uniform flexural rigidity (N/m), l the element length (m) and k_r the rail-pad stiffness (N/m).

Finally, the damping matrix of the generic i-th element depends only on the concentrated contribution of the railpad

$$[c]_i = c_r \cdot \begin{bmatrix} 1 & 0 & 0 & 0 \\ 0 & 0 & 0 & 0 \\ 0 & 0 & 1 & -0 \\ 0 & 0 & 0 & 0 \end{bmatrix}$$

Where c_r is the rail-pad dmping (N·s/m).

Appendix 2

The mass, damping and stiffness matrices are established imposing the vertical and rotational equilibrium of the bodies, which are the car body, the bogie and the wheelsets

$$[M] = \begin{bmatrix} M_c & 0 & 0 & 0 & 0 \\ 0 & M_t & 0 & 0 & 0 \\ 0 & 0 & J_t & 0 & 0 \\ 0 & 0 & 0 & M_w & 0 \\ 0 & 0 & 0 & 0 & M_w \end{bmatrix}$$

$$[C] = \begin{bmatrix} C_{s2} & -C_{s2} & 0 & 0 & 0 \\ -C_{s2} & C_{s2}+2C_{s1} & 0 & -C_{s1} & -C_{s1} \\ 0 & 0 & C_{s1}l_t^2 & -C_{s1}l_t & C_{s1}l_t \\ 0 & -C_{s1} & -C_{s1}l_t & C_{s1} & 0 \\ 0 & -C_{s1} & C_{s1}l_t & 0 & C_{s1} \end{bmatrix}$$

$$[K] = \begin{bmatrix} K_{s2} & -K_{s2} & 0 & 0 & 0 \\ -K_{s2} & K_{s2}+2K_{s1} & 0 & -K_{s1} & -K_{s1} \\ 0 & 0 & K_{s1}l_t^2 & -K_{s1}l_t & K_{s1}l_t \\ 0 & -K_{s1} & -K_{s1}l_t & K_{s1} & 0 \\ 0 & -K_{s1} & K_{s1}l_t & 0 & K_{s1} \end{bmatrix}$$

Where M_c is the car body mass (kg), M_t the bogie mass (kg), J_t the bogie pitch moment (kg·m^2), M_w the wheelset mass (kg), C_{s1} the primary suspension damping (N·s/m), C_{s2} the secondary suspension damping (N·s/m), l_t the distance between the centre of the bogie and the centre of the wheelset (m), K_{s1} the primary suspension stiffness (N/m) and K_{s2} the secondary suspension stiffness (N/m).